14th Australasian Fluid Mechanics Conference
Adelaide University, Adelaide, Australia
10-14 December 2001

The Impact of Strong Swirl and Buoyancy on the Structure of Turbulent Jets and Flames

W. Kollmann and I. M. Kennedy

Mechanical and Aeronautical Engineering Department
University of California, Davis, CA 95616, USA

Abstract

Jets and flames with strong swirl exhibit recirculation that leads to loss of axial momentum and a susceptibility to buoyancy forces for small Mach numbers. The impact of buoyancy on slightly heated, swirling jets and the effect of radiative heat loss on non-premixed, compressible, swirling flames are explored numerically.

Introduction

Jets with high Reynolds and Froude (Grashoff) numbers based on nozzle exit conditions are generally considered to be free of buoyancy effects. However, the presence of strong swirl can lead to the loss of axial momentum as a result of the induced pressure gradient, creating a stagnation point and recirculation. Under these conditions the jet may be very sensitive to buoyancy. The impact of buoyancy on the development of swirling jets is explored numerically. Compressible jet flames with swirl at nonzero Mach numbers are not affected by buoyancy, but the swirl changes the pressure field and soot reduces the internal energy. These effects are simulated for axi-symmetric, non-premixed ethylene-air flames.

Slightly heated jets

The slightly heated jet is incompressible except for the buoyancy force, which is approximated with the Boussinesq model. We consider only flows where the acceleration of gravity is aligned with the z-axis of the cylindrical coordinate system. A hybrid spectral finite-difference method was developed in [1], [2] to solve the Navier-Stokes equations in cylindrical coordinates. The azimuthal direction is discretized using the Fourier spectral collocation method (Canuto *et al.*,[3]). The dependent variables are the complex-valued Fourier amplitudes (k denotes the azimuthal wavenumber) for the azimuthal velocity, $\tilde{v}_\theta(k)$ $(k = 0, \cdots, N/2)$, the azimuthal vorticity $\tilde{\Omega}_\theta(k)$ $(k = 0, \cdots, N/2)$, the complex streamfunctions $\tilde{\Psi}(k)$ $(k = 0, \cdots, N/2)$, the complex pressure amplitudes $\tilde{p}(k)$ $(k = 1, \cdots N/2)$. The azimuthal velocity $\tilde{v}_\theta(k)$ is governed by

$$\frac{\partial \tilde{v}_\theta}{\partial t}(k) + \tilde{T}_\theta(k) = -i\frac{k}{r\rho}\tilde{p}(k) + \frac{1}{Re}\tilde{F}_\theta(k) \tag{1}$$

where $\tilde{T}_\theta$ are the convective terms, $\tilde{p}$ are the pressure modes and $\tilde{F}_\theta$ the viscous terms. The azimuthal vorticity $\tilde{\Omega}_\theta(k)$ satisfies

$$\frac{\partial \tilde{\Omega}_\theta}{\partial t} = -\tilde{T}^\Omega_\theta + \tilde{S}_\theta + \frac{1}{Re}\tilde{F}^\Omega_\theta + \frac{Gr}{Re^2}g_z\frac{\partial \tilde{T}}{\partial r} \tag{2}$$

where $\tilde{T}^\Omega_\theta$, $\tilde{S}_\theta$ are the convective and stretching terms and $\tilde{F}^\Omega_\theta$ the viscous terms. The Boussinesq model leads to the last term on the right side. The complex-valued stream functions $\tilde{\Psi}(k)$ are derived from the Fourier transformed mass balance, which implies that

$$d[r\tilde{\Psi}(r,k,z,t)] = -r\tilde{v}_z dr + r(\tilde{v}_r + ik\langle\tilde{v}_\theta\rangle)dz \tag{3}$$

is exact, hence

$$-r\tilde{v}_z = \frac{\partial}{\partial r}(r\tilde{\Psi}), \quad \tilde{v}_r + ik\langle\tilde{v}_\theta\rangle = \frac{\partial \tilde{\Psi}}{\partial z} \tag{4}$$

hold, where the angular brackets denote radial averaging,

$$\langle\Phi\rangle(r,k,z,t) \equiv \frac{1}{r}\int_0^r dr'\Phi(r',k,z,t) \tag{5}$$

The Helmholtz pdes for the streamfunctions are then given by

$$\tilde{\Omega}_\theta + ik\frac{\partial\langle\tilde{v}_\theta\rangle}{\partial z} = \frac{\partial}{\partial r}\left(\frac{1}{r}\frac{\partial}{\partial r}(r\tilde{\Psi})\right) + \frac{\partial^2\tilde{\Psi}}{\partial z^2} \tag{6}$$

The pressure modes $\tilde{p}(k)$ for $k = 1, \cdots, N$ are governed by

$$\begin{aligned}\frac{1}{r}\frac{\partial}{\partial r}(r\frac{\partial \tilde{p}}{\partial r}) - \frac{k^2}{r^2}\tilde{p} + \frac{\partial^2\tilde{p}}{\partial z^2} &= -\rho\frac{Gr}{Re^2}g_z\frac{\partial\tilde{T}}{\partial z}\\ &-\rho\mathcal{F}_N[(\frac{\partial v_r}{\partial r})^2 + \frac{1}{r^2}(\frac{\partial v_\theta}{\partial\theta} + v_r)^2 + (\frac{\partial v_z}{\partial z})^2\\ &+\frac{2}{r}\frac{\partial v_\theta}{\partial r}(\frac{\partial v_r}{\partial\theta} - v_\theta) + 2\frac{\partial v_r}{\partial z}\frac{\partial v_z}{\partial r} + \frac{2}{r}\frac{\partial v_z}{\partial\theta}\frac{\partial v_\theta}{\partial z}]\end{aligned} \tag{7}$$

containing a buoyancy contribution. The dimensionless groups, Grashoff and Reynolds numbers, are defined by

$$Gr \equiv \frac{\beta\triangle TgL}{U^2}, \quad Re \equiv \frac{UL}{\nu} \tag{8}$$

where β denotes the thermal expansion coefficient and ν the kinematic viscosity, $\triangle T$ is the temperature difference between jet fluid and the environment (typically less than ten degrees Celsius) and U, L are velocity and length scales. Axi-symmetric flows are simulated by restricting the wavenumber range to $k = 0$, hence no pressure modes are required.

The equations for the Fourier modes are dicretized with respect to radial and axial directions with uniform spacing in the image domain $[0, 1] \times [0, 1]$. Either central differences are used for first and second derivatives with explicit filters (Kennedy & Carpenter [4], applied to the increments of the transport equations) or upwind-biased differences (Li[5]) for the convective terms and central differences for the other derivative terms. The filter order is chosen such that it does not degrade the accuracy of the finite-difference schemes, no filters are applied for the upwind-biased schemes.

The time integrator is an explicit 4^{th}-order state space Runge-Kutta method that requires minimal storage as

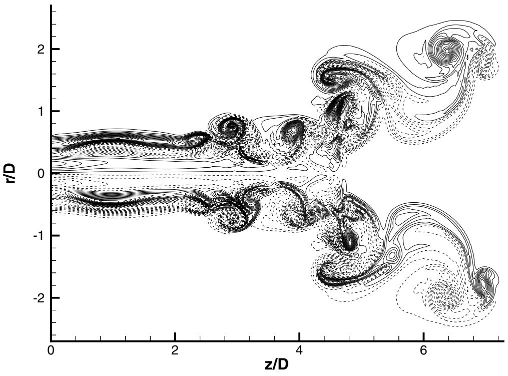

Figure 1: Iso-lines of enstrophy for $Re = 2500$, $S = 1.41$, $Gr/Re^2 = 0.16$ at $t = 22.8$. The jet is oriented upward ($g_z = -1$).

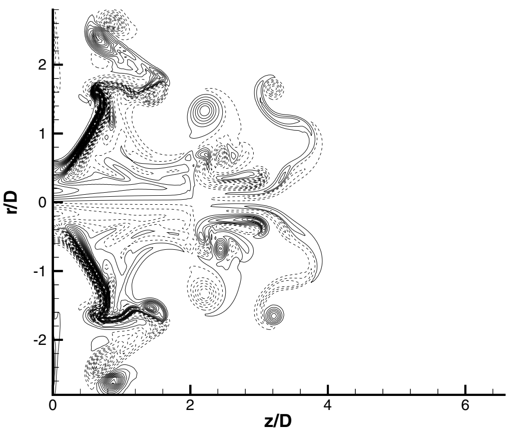

Figure 2: Iso-lines of enstrophy for $Re = 2500$, $S = 1.41$, $Gr/Re^2 = 0.05$ at $t = 22.8$. The jet is oriented downward ($g_z = 1$).

described in [1]. The Helmholtz equations for the streamfunction and pressure modes are solved using LU-decomposition combined with deferred corrections to reduce the bandwidth of the coefficient matrix.

All simulations are done with the fifth order upwind-biased and fourth order central solver. The axi-symmetric swirling jets with buoyancy are computed with $Gr/Re^2 = 0.16$ for the upward orientation ($g_z = -1$) and with $Gr/Re^2 = 0.05$ for the downward ($g_z = 1$) orientation. The swirl number is according to [6] defined by

$$S \equiv \frac{2v_\theta(R/2, z_0)}{v_z(0, z_0)} \tag{9}$$

where $z_0 = 0.4D$, $D = 2R$ being the nozzle diameter. The results for the upward and downward direction of the jet axis for $Re = 2500$ and $S = 1.41$ are shown in fig.1 to 2. Buoyancy modifies the vortical structure of the swriling jets drastically. The conical jets near the entrance have opening angles different by an order of magnitude due to buoyant transport of vorticity. Unfortunately, no relevant experimental data are available on heated swirling jets for comparison; experiments are currently under way at UC Davis.

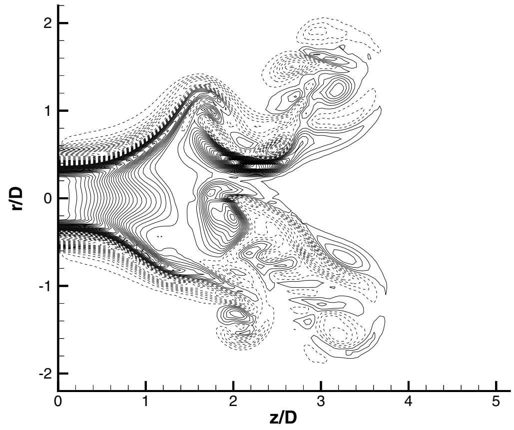

Figure 3: Cross-section of the Iso-surfaces of Ω_z at $\theta = 0$ (upper half) and $\theta = \pi$ (lower half) for $Re = 1000$, $S = 1.35$ at $t = 15.1$ and zero gravity, fully 3-d simulation.

The fully 3-d simulation for $Re = 1000$ and $S = 1.35$ in fig.3 and fig.4 at zero gravity shows the expected spreading of the conical jet observed in the experiments [6]. The vortex interactions are quite different from the axi-symmetric case due to realignment of vortex ring structures and the creation of helical counter-rotating vortex braids.

Compressible flames

Compressible flames at moderate Mach numbers of the order 0.3 are not affected by buoyancy and the simulations are done at zero gravity. However, the effect of swirl, when coupled with a highly non adiabatic flow field as a result of radiation, can lead to unique flow structures. The compressible Navier-Stokes equations in cylindrical coordinates using the primitive variables are set up in dimensionless form for axi-symmetric flows. The solver is based on fourth order central difference operators and high order filters to provide the numerical dissipation to stabilize the system (Kennedy and Carpenter [4]). A fourth order Runge-Kutta type time integration method with an embedded third order scheme to monitor and control the time integration error and with minimal storage requirements (Kennedy and Carpenter [4]) is implemented.

The solver includes additional pdes for mixture fraction and soot volume fraction to deal with combustion and the formation and transport of soot. The combustion reactions are simplified assuming that all chemical components are ideal gases and the mass diffusivities are equal and constant. The flame sheet model is defined by the requirement that the Gibbs free energy is a minimum for a given state. The state is defined in terms of pressure, temperature and composition variables and the minimum is computed using STANJAN. These variables are determined indirectly by prescribing density ρ, internal energy u and mixture fraction Z in a range suitable for the flames considered and using thermodynamic relations to set up

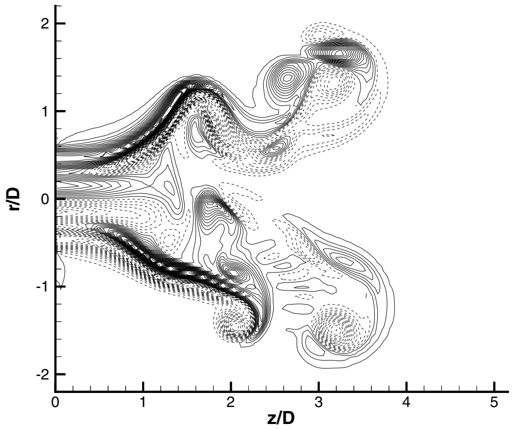

Figure 4: Cross-section of the Iso-surfaces of Ω_θ at $\theta = 0$ (upper half) and $\theta = \pi$ (lower half) for $Re = 1000$, $S = 1.35$ at $t = 15.1$ and zero gravity, fully 3-d simulation.

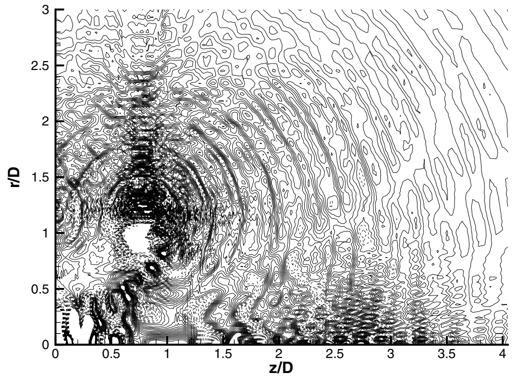

Figure 5: Isobars (disturbance pressure $(p - p_0)/\rho_0 U_0^2$) for $Re = 1500$, $S = 1.31$ at $t = 5.8$ in a non-premixed ethylene-air flame. The isobars shown are equally spaced in $[-0.25, 0.25]$ where $p_{max} = -0.96887$ and p_{min} =0.93722

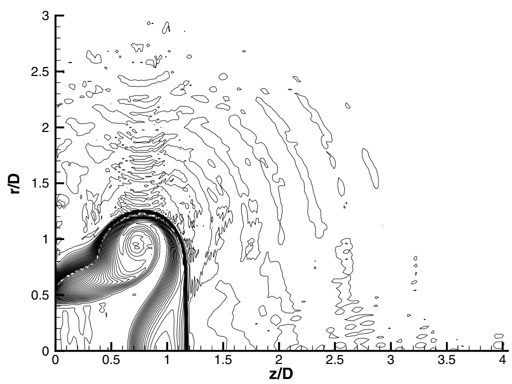

Figure 6: Isotherms for $Re = 1500$, $S = 1.31$ at $t = 5.8$ in a non-premixed ethylene-air flame.

the input to STANJAN. Mixture fraction Z is defined by considering the reaction of the hydrocarbon fuel C_nH_m with air in a single step

$$C_nH_m + (n + \frac{1}{4}m)O_2 + (n + \frac{1}{4}m)bN_2 \leftrightarrow nCO_2$$

$$+\frac{1}{2}mH_2O + (n + \frac{1}{4}m)bN_2 \tag{10}$$

The composition of pure air is given by Y_i^∞ (Y_i denotes mass fraction) and $b \equiv Y_{N_2}^\infty / Y_{O_2}^\infty$. A coupling function (Williams [8], sect.3.4.2) denoted by β can be used to define mixture fraction

$$Z = \frac{\beta - \beta^\infty}{\beta^0 - \beta^\infty} \tag{11}$$

where β_0 and β_∞ denote the values at the entrance section and in the free stream; β can be constructed by ($F = C_nH_m$)

$$\beta = \frac{Y_F}{M_F \nu'_F} - \frac{Y_{O_2}}{M_{O_2} \nu'_{O_2}} \tag{12}$$

which is conserved in the limit of infinite reaction rate. The results of the equilibrium computations are tabulated and the solver determines the local state using a combined linear and cubic spline interpolation in the table. The compressible flame sheet model consists of mass balance, which determines ρ, the energy balance for the internal energy u and the convection-diffusion equation for mixture fraction Z plus the ideal gas equation determining the pressure. The local thermodynamic state is thus determined by two independent intensive variables, density ρ and internal energy u, plus composition via the mixture fraction Z consistent with the state principle.

The complexity of the compressible Navier-Stokes solver precludes, for the time being, the use of two equation soot models, such as that of Syed et al.[9], or complex models that include detailed chemistry (Frenklach and Wang[10]). Hence, the simple model that was proposed by Kennedy et al.[7] for soot formation in an ethylene flame has been adopted. It adds one pde for the soot volume fraction to the system of equations and specifies the divergence of the radiative heat flux in the energy equation through the assumption of optical thinness. The additional pde for the soot volume fraction Φ is given by

$$\frac{\partial}{\partial t}(\rho\Phi) + \frac{\partial}{\partial r}(\rho\Psi v_r) + \frac{1}{r}[\frac{\partial}{\partial \theta}(\rho\Phi v_\theta) + \rho\Phi v_r]$$

$$+\frac{\partial}{\partial z}(\rho\Phi v_z) = \frac{1}{ReSc^s}\left\{\frac{\partial}{\partial r}(\rho\frac{\partial\Phi}{\partial r}) + \frac{\partial}{\partial z}(\rho\frac{\partial\Phi}{\partial z})\right.$$

$$\left.+\frac{1}{r}[\frac{1}{r}\frac{\partial}{\partial\theta}(\rho\frac{\partial\Phi}{\partial\theta}) + \rho\frac{\partial\Phi}{\partial r}]\right\} + \rho(Q_n + Q_g - Q_o) \tag{13}$$

where Sc^s denotes the Prandtl/Schmidt number for the soot volume fraction. Thermophoresis was not included as it is negligible for the present flames. The diffusivity of soot is only a fraction of the gas diffusivity, hence $Sc^s = 10Sc$ was set for the simulations. The source and sink terms account for the formation and oxidation processes of soot, $Q_n(Z)$ determines the amount of soot created by particle nucleation, $Q_g(Z, T, \Phi)$ the amount produced by surface growth and $Q_o(Z, T, \Phi)$ is the destruction rate of soot by oxidation. Oxidation by OH has not been included in this formulation as a result of the use of a

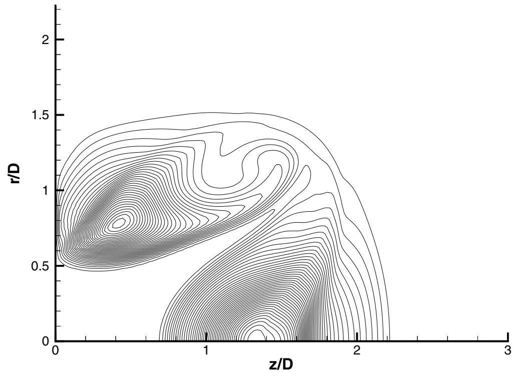

Figure 7: Isolines of soot volume fraction Φ for $Re = 1500$, $S = 1.41$ at $t = 5.8$ in a sooting non-premixed ethylene-air flame.

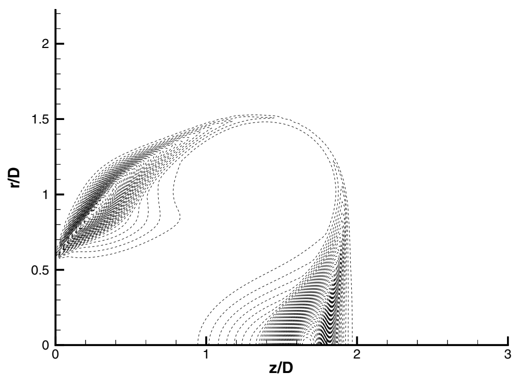

Figure 8: Isolines of the radiative sink in the energy equation for $Re = 1500$, $S = 1.41$ at $t = 5.8$ in a sooting non-premixed ethylene-air flame.

simple thermodynamic model. The explicit form of these semi-empirical models can be found in Kennedy et al.[7].

The divergence of the radiative flux vector in the energy balance is according to the model of Kennedy et al.[7] given (dimensional form) by

$$\nabla \cdot \mathbf{q}^R = 8\pi K_1 \rho \Phi^{\frac{2}{3}} [1 - (\frac{T_\infty}{T})^4] \int_0^\infty \frac{d\lambda}{\lambda^6 [\exp(\frac{C_2}{\lambda T}) - 1]} \quad (14)$$

where $K_1 = 4.16808\ 10^{14}$, $T_\infty = T_0$ and $C_2 = 14388 \mu m K$. The divergence of the radiative flux is made dimensionless with its value at the adiabatic flame temperature.

The results for a swirling, axi-symmetric, non-premixed flame burning ethylene with air at a Mach number $M_0 = 0.3$ and the Reynolds number $Re = 1500$ are shown in fig.5 to 8. The disturbance pressure field in fig.5 and the temperature in fig.6 indicate the waves emanating from the flame wrapped around the starting vortex. Soot volume fraction in fig.7 and the radiative sink (14) in fig.8 are insignificant in the high stretch region of the flame.

Conclusions

A hybrid spectral-finite difference method is used for the simulations of the slightly heated jets for axi-symmetric and fully 3-d flows. The results for the swirling jet oriented upward and downward show a significant dependence of the vorticity distributions on the direction of gravity. The opening angle of the conical jet section of the swirling jets differs by more than a hundred percent for the upward and downward directions.

The swirling compressible flame based on an equilibrium flame sheet model for the combustion of ethylene with air was run at zero gravity for a Mach number $Ma = 0.3$ and a Reynolds number $Re = 1500$ for the axi-symmetric case only. The results show a strong effect of swirl on the distribution of soot in the flame. Acoustic waves are generated near the flame tip produce a complex pressure field, that modifies the flame temperature. Swirl is found to play a major role in the development of turbulent jets, reacting and non reacting. The presence of a stagnation point in the latter flows leads to a strong impact of buoyancy on flow structure. The impact of swirl on mixing, and hence on soot formation and radiation in the former case, also has a major impact on flow development.

References

[1] W. Kollmann and J.Y. Roy (2000), "Hybrid Navier-Stokes solver in cylindrical coordinates I: Method", Computational Fluid Dynamics Journal **9**, 1-16.

[2] W. Kollmann and J.Y. Roy (2000), "Hybrid Navier-Stokes solver in cylindrical coordinates II: Validation", Computational Fluid Dynamics Journal **9**, 17-22.

[3] Canuto, C., Hussaini, M.Y. and Zang, T.A. (1988), "Spectral Methods in Fluid Dynamics", Springer-Verlag, Berlin.

[4] C.A. Kennedy and M.H. Carpenter (1994), "Several new numerical methods for compressible shear layer simulations", Appl. Num. Math. **14**, 397-433

[5] Li, Y. (1997), "Wavenumber Extended High-Order Upwind-Biased Finite Difference Schemes for Convective Scalar Transport", *J. Comput. Phys.* 133: 235-255.

[6] P. Billant, J. Chomaz and P. Huerre (1999), "Experimental study of vortex breakdown in swirling jets", *J. Fluid Mech*, 376: 183-219.

[7] Kennedy, I.M., Kollmann, W. and Chen, J.-Y. (1990), "A Model for Soot Formation in a Laminar Diffusion Flame", Combust. Flame **81**, 73-85.

[8] Williams, F.A. (1985), "Combustion theory", Benjamin/Cummings Inc., Menlo Park, CA.

[9] Syed, K.J., Stewart, C.D. and Moss, J.B. (1990), "Modeling soot formation and thermal radiation in buoyant turbulent diffusion flames", 23rd Symposium (Int.) on Combustion, The Combustion Institute, Pittsburgh PA, 1533-1541.

[10] Frenklach, M. and Wang, H. (1994), "Detailed Mechanism and Modeling of Soot Formation", in *Soot Formation in Combustion* (H. Bockhorn ed.), Springer Verlag, Berlin, 162-190.